Integrated processing of contrast pulse sequencing ultrasound imaging for enhanced active contrast of hollow gas filled silica nanoshells and microshells

Casey N. Ta[a)]
University of California, San Diego, Department of Electrical and Computer Engineering, 9500 Gilman Drive Mail Code 0407, La Jolla, California 92093

Alexander Liberman[a)]
University of California, San Diego, Materials Sciences and Engineering Program, 9500 Gilman Drive Mail Code 0418, La Jolla, California 92093

H. Paul Martinez
University of California, San Diego, Department of Chemistry and Biochemistry, 9500 Gilman Drive Mail Code 0358, La Jolla, California 92093

Christopher V. Barback
University of California, San Diego, Department of Radiology, 200 W Arbor Drive, San Diego, California 92103

Robert F. Mattrey
University of California, San Diego, Medical Center, MRI Institute, Department of Radiology, 410 Dickinson Street, San Diego, California 92103 and University of California, San Diego, Moores Cancer Center, 3855 Health Sciences Drive, La Jolla, California 92093

Sarah L. Blair
University of California, San Diego, Department of Surgery, UCSD, 200 W. Arbor Drive, San Diego, California 92103 and University of California, San Diego, Moores Cancer Center, 3855 Health Sciences Drive, La Jolla, California 92093

William C. Trogler and Andrew C. Kummel
University of California, San Diego, Department of Chemistry and Biochemistry, 9500 Gilman Drive Mail Code 0358, La Jolla, California 92093

Zhe Wu[b)]
University of California, San Diego, Department of Radiology, 200 W Arbor Drive, San Diego, CA 92103 and University of California, San Diego, Moores Cancer Center, 3855 Health Sciences Drive, La Jolla, California 92093

(Received 15 January 2012; accepted 1 March 2012; published 23 March 2012)

In recent years, there have been increasing developments in the field of contrast-enhanced ultrasound both in the creation of new contrast agents and in imaging modalities. These contrast agents have been employed to study tumor vasculature in order to improve cancer detection and diagnosis. An in vivo study is presented of ultrasound imaging of gas filled hollow silica microshells and nanoshells which have been delivered intraperitoneally to an IGROV-1 tumor bearing mouse. In contrast to microbubbles, this formulation of microshells provided strong ultrasound imaging signals by shell disruption and release of gas. Imaging of the microshells in an animal model was facilitated by novel image processing. Although the particle signal could be identified by eye under live imaging, high background obfuscated the particle signal in still images and near the borders of the tumor with live images. Image processing techniques were developed that employed the transient nature of the particle signal to selectively filter out the background signal. By applying image registration, high-pass, median, threshold, and motion filtering, a short video clip of the particle signal was compressed into a single image, thereby resolving the silica shells within the tumor. [http://dx.doi.org/10.1116/1.3694835]

I. INTRODUCTION

Over the past several decades substantial improvements have been made in the development of ultrasound contrast agents. Overwhelmingly, these contrast agents consist of polymeric, protein, or phospholipid formulations, which form shells around encapsulated perfluorocarbon gas or air.[1–3] These contrast agents can be imaged with the use of ultrasound by either detecting the characteristic harmonic oscillations of microbubbles or destroying the microbubbles to generate a broadband signal.[2–4] In both cases, it is possible to generate signal because of the substantial acoustic impedance mismatch between the gas and the surrounding environment.[1,4] Typically, ultrasound contrast agents are administered intravenously to study vasculature; due to the typical size of the

[a)]Authors contributed equally to this work.
[b)]Electronic mail: zhewu@ucsd.edu

microbubbles (1–5 μm), they cannot escape the vasculature.[2–6] Consequently, ultrasound contrast agents have been employed frequently in the detection and diagnosis of tumors by studying aberrant tumor vasculature due to angiogenesis.[4,7–10]

Recent innovations and advancements in ultrasound contrast agents have stimulated development of enhanced methods to image these agents in order to increase image contrast and quality. Notably, contrast pulse sequencing (CPS) imaging has found widespread application by optimizing the waveform used to discriminate against the linear signal response typically seen in tissues and emphasize nonlinear signals generated by microbubble contrast agents.[3,11,12] With these techniques, it is possible to suppress or eliminate the signal from the tissue while displaying the signal from the contrast agents. This allows substantial contrast to be achieved with various commercial contrast agents, such as Definity, Sonovue, and Sonazoid.[12]

Although microbubble contrast agents and contrast-enhanced ultrasound (CEUS) imaging techniques generally provide specific imaging of the microbubbles, image processing steps can provide additional image enhancement. Dave *et al.* combined cumulative maximum intensity and a sum of absolute differences motion filter to subharmonic images of contrast agents to create single images with complete traces of tumor vasculature.[13] Ching-Hsiang *et al.* applied a sequence of image processing steps including high-pass filter, thresholding, medium filter, motion filter, and summation to B-mode images of contrast agents to detect permeability of the blood brain barrier.[14] Aside from image enhancement purposes, many researchers apply image processing techniques to quantify tumor blood flow or to create parametric images displaying the kinetic information with a color map for diagnostic or therapeutic purposes.[15–18]

Hollow silica particles have been explored recently as ultrasound contrast agents. Lin *et al.* tested hollow silica capsules with CPS at high MI in a liquid filled plastic beaker.[19] Martinez *et al.* employed color Doppler imaging to selectively image gas-filled silica nanoshells and microshells in tissue phantoms and in excised mastectomy tissue.[20] However, these were nonliving samples with no blood flow, which could obfuscate the Doppler signal from the particles. Hu *et al.* developed hollow silica microspheres that were imageable at low MI (0.06) and injected them into male rat spermary and imaged with CEUS.[21] Although background tissue signal was present, the high local concentration of particles was readily detectable by eye.

In this study, the imaging mechanism of hollow silica nanoshells and microshells were first examined *in vitro*. Previously, the use of hollow silica nanoshells and microshells as stationary markers using color Doppler ultrasound imaging *in vitro* was reported.[20] For marking tumors for surgical excision (e.g., breast conservation therapy) via injection of silica nanoshells and microshells, only stationary imaging is required. However, for locating tumors not localized by other modalities, such as CT, systemic injection may be useful. Unfortunately, it is impossible to selectively image these hollow silica nanoshells and microshells in circulation using color Doppler due to the substantial color Doppler signal present from blood flow. To study the imaging behavior in circulation *in vivo*, high mechanical index (MI) CPS was used to image perfluoropentane filled hollow nanoshells and microshells delivered intraperitoneally to an IGROV-1 tumor bearing mouse model. The systemic delivery of gas-filled silica contrast agents, as performed in this report, presented a difficult problem in terms of imaging. Selectively imaging the particles proved challenging due to the increased nonlinear tissue response under high MI and the infrequent signal response from the injected particles. The focus of this study was to develop image processing techniques that filter the background tissue signal from the particle response and thereby form a clear image of the tumor.

II. MATERIALS AND METHODS

A. Silica particle fabrication

Tetramethyl orthosilicate (TMOS), trimethyl borate (TMB), perfluoropentane (PFP), and 0.1|% poly-L-lysine (PLL) were purchased from Sigma Aldrich (St. Louis, MO). Polystyrene templates were purchased from Polysciences (Warrington, PA). Phosphate buffered solution (PBS) was purchased from Fisher Scientific (Pittsburgh, PA). Silica microshells and nanoshells were produced and filled with perfluoropentane gas as previously described by Martinez *et al.*[20] The microshells and nanoshells were suspended at a concentration of 2 mg/ml after gas filling with perfluoropentane (PFP) and stored at room temperatures. Particles were examined with SEM to ensure size consistency and shell formation. A bolus of 100 μl of particles were administered IP to the mice and then imaged hourly.

B. Examination of hollow silica particle imaging mechanism

The Siemens Acuson Sequoia 512 Ultrasound machine (Siemens Medical Solutions, Mountain View, CA) was used throughout with the Acuson 15L8 transducer. During imaging of particles, wall filters and gains were optimized in order to maximize signal from particles while reducing background. Initial imaging experiments were conducted on the 2 μm gas filled shells diluted to 0.1 mg/ml. Particles were inserted into a thin wall acoustically transparent chamber and clamped in a water bath. The 15L8 transducer of the Siemens Sequoia was clamped in the water bath perpendicular to the sample such that the bulb carrying the sample could be imaged clearly. The particles were imaged with contrast pulse sequencing (CPS) at various mechanical indices to assess particle response to ultrasound imaging.

Since the silica particles have rigid shells, unlike the compressible microbubble contrast agents, it was speculated that high MI CPS was able to successfully image these particles by rupturing the shells, thereby releasing PFP gas and creating local decorrelation events in the received ultrasound signal. To further investigate the mechanism of imaging, 500 nm and 2 μm particles were placed into an acoustically transparent chamber and subjected to high intensity focused ultrasound (HIFU) for 2 min. Particles were recovered from the chamber and were imaged with a scanning electron microscope (SEM) to determine shell integrity following imaging.

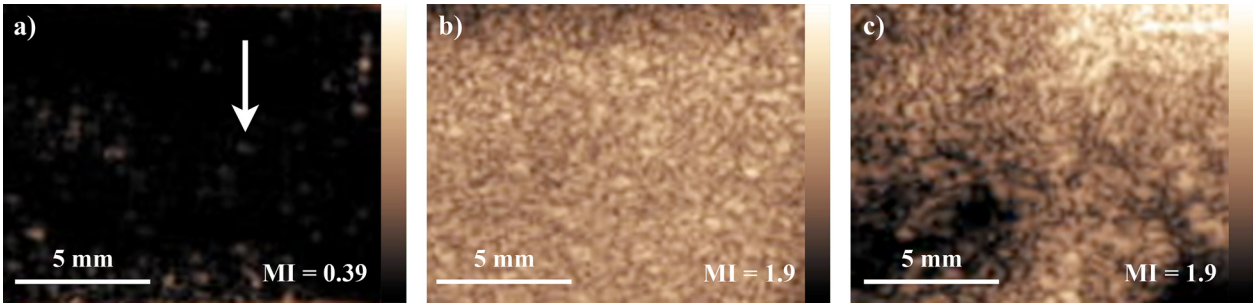

FIG. 1. (Color online) CPS Imaging of Gas Filled Silica Microshells. 100 μg/ml of gas filled 2 μm silica microshells were imaged in a thin-walled acoustically transparent chamber using CPS mode. (a) CPS image of microparticles at 0.39 MI. Each bright spot was a single imaging event; the white arrow points to a single imaging event. At low MI, the received signal intensity from each imaging event was low, resulting in dim images where the particle signal may be difficult to observe. (b) CPS image of microparticles at 1.9 MI. The large density of bright spots corresponded to a large number of particles being imaged. The received signal intensity was much stronger than at low MI, resulting in much brighter images. (c) CPS image of traditional microbubbles at a concentration of 10^8 microbubbles/ml which closely correlated in particle count to 100 μg/ml of the silica microshells.

C. *In vivo* CPS imaging of silica particles

A mouse ovarian tumor model was employed to study the imaging behavior of the particles delivered via intraperitoneal (IP) injection. Two five-week-old female nu/nu mice (Charles River Laboratories, Wilmington, MA) were housed in a UCSD approved animal housing facility at 22 °C with a 12 h light/dark cycle. After an acclimation period of ten days, 10^6 IGROV-1 cells were injected IP and developed large malignant tumors within 5 weeks. Prior to particle delivery, excess fluid was drained from the peritoneal cavity to reduce excess fluid pressure and reduce the likelihood of particles leaking out of the needle tract. 200 μg of PFP filled 2 μm or 500 nm particles (data not shown) were diluted in 3 ml of saline were injected IP; IP injections have been previously used as a form of systemic delivery in mouse models.[22–24] During particle administration and imaging the mice were anesthetized with isoflurane gas. The tumors were imaged at high MI using CPS imaging one hour after injection. After imaging, mice were anesthetized with isoflurane gas and sacrificed by CO_2 asphyxiation.

D. Image processing

Image processing routines, as described in Sec. III B below, were implemented in MATLAB R2011a. Processing was performed on a laptop with an Intel Core i7–2720QM processor, 6 GB of RAM, and a NVIDIA GeForce GT 525M GPU. The image processing code was single threaded and was not optimized for speed. Image registration was the most time consuming step, requiring up to 30 min per video analyzed. The remaining processing steps required less than 1 min to complete. Processing times can potentially be significantly reduced by using faster image registration routines[25] and general purpose GPU (GPGPU) programming.[26–28]

III. RESULTS AND DISCUSSION

A. Examination of silica particle imaging mechanism

Unlike the commercially available microbubble contrast agents, the gas-filled silica particles have rigid, uncompressible shells. However, these particles can be ruptured (evidence shown in Fig. 2), causing local decorrelation events which appeared as bright, circular spots on the CPS image. Figure 1 shows the results of imaging the 2 μm particles at (A) 0.39 MI and (B) 1.9 MI with CPS. As expected, the particle bursting resulted in bright spots which were associated with isolated US echo decorrelation events. At 0.39 MI, only a light density of spots appeared in the CPS image, but as the MI was increased to 1.9, the density of bright spots increased dramatically. This observation was consistent with the mechanism of imaging by shell rupture; at low MI (0.39), the ultrasound pressure was only strong enough to fracture the mechanically weaker particles, resulting in a dimmer image, whereas at high MI (1.9), the pressure could rupture many particles simultaneously, resulting in a brighter image. Figure 1(c) contains a CPS image of traditional microbubbles (Definity) at a concentration of 10^8 microbubbles/ml imaged at 1.9 MI. Comparing Figs. 1(b) and 1(c), it was shown *in vitro* that the silica microshells provided a comparable

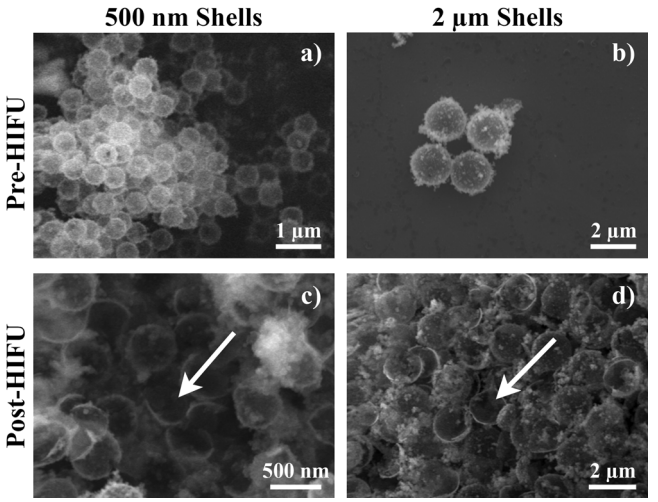

FIG. 2. SEM images of particles preand post-HIFU. Scanning electron microscopy (SEM) images of (a) 500 nm and (b) 2 μm particles after synthesis but before receiving any treatment or experimentation. SEM images of (c) 500 nm and (d) 2 μm particles after undergoing 2 min of high intensity focused ultrasound (HIFU). The appearance of semispherical half-shells (white arrows) only after HIFU was consistent with the assumption that the particles were fractured during high mechanical index imaging.

amount of contrast relative to commercially available contrast agents at high MI.

To confirm that the silica particles were being ruptured under high pressure US, the 500 nm and 2 μm particles were exposed to HIFU for 2 min and imaged with SEM. Prior to HIFU, the silica particles appeared as highly monodisperse spheres [Figs. 2(a) and 2(b)]. After exposure to HIFU, the particles appeared as a mixed population of intact spheres and semispherical halves (Figs. 2(c) and 2(d), white arrows), confirming the hypothesis that the gas-filled shells were being fractured during imaging. Additionally, it has been previously established that the shell thickness to particle radius ratio has substantial effect on the mechanical properties of the particles.[29] The thicknesses of the shells for both sizes were approximately the same, but the radii were not, resulting in the 500 nm shells being mechanically stronger and showing fewer fragmented shells post-HIFU.

B. *In vivo* CPS imaging and image processing

The 2 μm gas filled silica particles were tested *in vivo* with an IGROV-1 mouse ovarian tumor model. The particles were injected intraperitoneally; IP injections have been used previously as a form of systemic delivery in mouse models.[22–24] One hour post-injection, the tumor was imaged with dual B-mode and CPS imaging at high MI. Signal from the silica microshells was readily identified under live imaging by a few characteristic properties (Fig. 3). Signal from the particles appeared mostly within the tumor as bright, isolated, circular spots (green arrows) associated with particle destruction events. The signal from each destruction event was transient and persisted for only 1–3 frames. However, under high MI, tissue behaves more nonlinearly and significant levels of background signal were generated by the tissue, making it difficult to distinguish particle signal from background signal in still images. Furthermore, since the destruction imaging events were sparse and scattered over time, a full image of the tumor could not be seen from a single image.

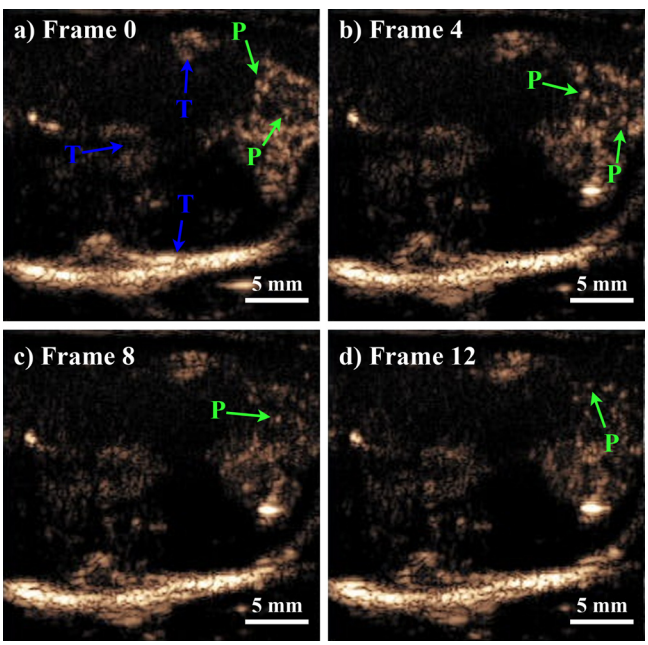

FIG. 3. (Color online) *In vivo* Silica Particle CPS Imaging. CPS imaging was performed 1 h after IP injection of 2 μm gas filled silica particles in a mouse tumor model. A sample of frames were chosen, each frame sequentially four frames apart, to show that (1) the particle signal appeared as transient bright spots (P: green arrows) and (2) under high MI CPS imaging, there was significant nonlinear tissue response that persisted over time (T: blue arrows).

To improve the imaging of the silica particles, the CEUS imaging processing was performed in four steps.

(1) Image registration was performed first to correct motion due to movement of the transducer and breathing of the mouse, providing a stable spatial frame of Ref. 30. The rigid image registration parameters were detected from the B-Mode images and applied to the CPS images.
(2) Capitalizing on the transient nature of the particles, a high-pass filter (HPF) was applied to reduce the majority of the signal response from the background tissue.[31]
(3) A median filter and threshold filter were applied to remove individual pixels and low intensity signals.[32] However, motion perpendicular to the imaging plane could not be corrected by image registration and introduced changes to the tissue structure (and thus the background signal) which could pass through all of the above processing steps.
(4) The sum of squared differences between sequential frames was used to detect motion from frame to frame, and the particle signals from these frames were filtered out (i.e., a global motion filter).

Since only several particle destruction events were visible in any given frame, to produce an image with a clear depiction of the entire tumor, the particle signal was integrated over all frames and collapsed into a single image rendered as a red-yellow heat map superimposed on the gray scale B-mode image (Fig. 4). To demonstrate the effectiveness of each of the processing steps, Fig. 4 shows the resultant integrated intensity heat map when each of the steps were added to the processing pipeline. The curved, horizontal feature near the bottom of the images was the back of the mouse which strongly reflected the ultrasound signal, and the green arrow in Fig. 4(d) shows the location of the tumor. When only motion correction was applied [Fig. 4(a)], the signal reflecting from the back of the mouse was much stronger than the particle signal from the tumor. When the high-pass filter was applied [Fig. 4(b)], the signal reflecting from the back of the mouse was reduced to a level comparable to the signal coming from the tumor. Note that relative to Fig. 4(a), Fig. 4(b) appears brighter because the color scale in each image was normalized to the most intense signal within the image. After the median and threshold filters were applied [Fig. 4(c)], the majority of the background signal was eliminated, and the edges of the tumor could be seen clearly, but the tumor signal was still comparable to the reflected signal. Finally, with the global motion filter [Fig. 4(d)], the particle signal from the tumor became the dominant signal within the image, allowing signal generated by the particles to be clearly imaged within the tumor 1 h after injection.

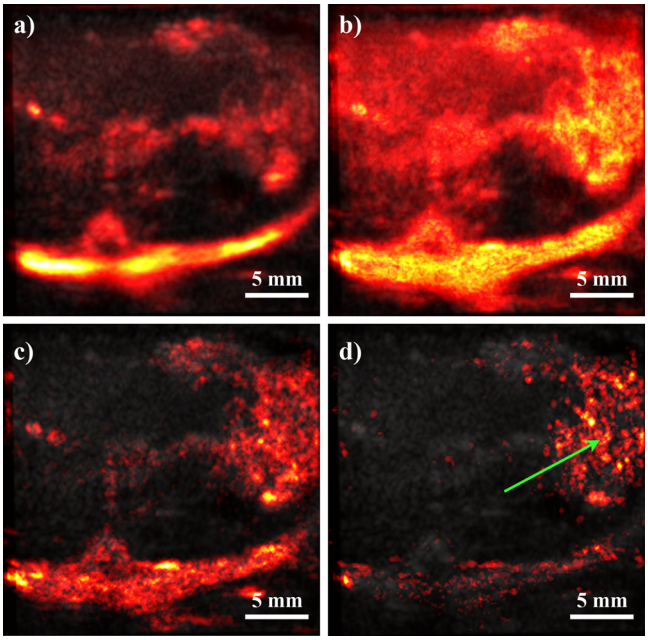

FIG. 4. (Color online) Microparticle The images shown above illustrate the change of the integrated intensity of the CPS image signal after image processing steps were incrementally added: (a) MC, (b) MC + HP filter, (c) MC + HP + M&T filters, and (d) MC + HP + M&T + GM filters. In each image, the particle signal was rendered as a heat map overlaid on a grayscale B-mode background. Each heat map was normalized such that the brightest signal within each image appears white. The green arrow points to the tumor. As each image processing step was added from (a)–(d), the tumor signal became increasingly dominant relative to background tissue signal. MC: motion correction, HP: high-pass filter, M&T: median and threshold filter; GM: global motion filter.

IV. SUMMARY AND CONCLUSIONS

This study investigated the imaging of perfluoropentane filled silica nanoshells and microshells and presented a novel image processing technique to selectively image systemically delivered particles. While a previous study showed that stationary perfluoropentane filled silica nanoshells and microshells could be readily imaged by color Doppler US, imaging when particles are in motion requires a different US imaging technique and different signal processing. These particles were shown to selectively image a tumor in a mouse ovarian tumor model via intraperitoneal injection of the particles. Although background tissue response significantly dominated over the particle signal under high MI CPS imaging, custom image processing steps were designed which took advantage of the transient characteristics of the particle signal to filter out the background tissue response. The short persistence of the particle signal allowed the high-pass filter to remove background tissue signal without affecting the particle signal. Capitalizing on the high intensity and circular spot shape of the particle signal, the median and threshold filters provided synergistic effectiveness with the HPF by eliminating the individual pixels and low intensity background signal that survived the HPF. Although the particle signal was slightly diminished by the motion filter, this final processing step eliminated most of the motion-induced signal and provided an image where the particle signal within the tumor could be identified precisely. Although other researchers have investigated using hollow silica particles as ultrasound contrast agents, including Hadinoto *et al.*,[29] Lin *et al.*,[19] Martinez *et al.*,[20] and Hu *et al.*,[21] this is the first report to the authors' knowledge of applying image processing techniques to selectively retain the signal response from systemically delivered silica particles. The image processing routines developed here may also be beneficial to other researchers investigating the use of rigid-shelled gas-filled particles as ultrasound contrast agents.

ACKNOWLEDGMENTS

This study utilized the Small Animal Imaging Resource supported by the *In vivo* Cancer and Molecular Imaging Center (ICMIC) P50-CA128346. C.T. and A.L. were supported by an R25 CA153915 Center for Cross Training Translation Cancer Researcher in Nanotechnology (CRIN) training grant and R01 CA095298. Z.W. was supported by a Career Development Award through the ICMIC. The authors wish to thank Siemens Medical Solutions USA, Inc. for providing the Acuson Sequoia 512 US system as an equipment loan to UCSD.

[1]D. Cosgrove, Eur. J. Radiol. **60**, 324 (2006).
[2]S. Qin, C. F. Caskey, and K. W. Ferrara, Phys. Med. Biol. **54**, R27 (2009).
[3]K. Ferrara, R. Pollard, and M. Borden, *Annual Review of Biomedical Engineering* (Annual Reviews, Palo Alto, 2007), Vol. 9, pp. 415–447.
[4]K. W. Ferrara, C. R. B. Merritt, P. N. Burns, F. Stuart Foster, R. F. Mattrey, and S. A. Wickline, Acad. Radiol. **7**, 824 (2000).
[5]M. A. Borden, and M. L. Longo, Langmuir **18**, 9225 (2002).
[6]E. Leen, S. J. Moug, and P. Horgan, Eur. Radiol. **14**, P16 (2004).
[7]F. G. Balen, C. M. Allen, and W. R. Lees, Clin. Radiol. **49**, 77 (1994).
[8]X. Q. Dong, Y. Shen, L. W. Xu, C. M. Xu, W. Bi, and X. M. Wang, Chin. Med. J. (Engl). **122**, 1179 (2009).
[9]H. Marret, S. Sauget, B. Giraudeau, M. Brewer, J. Ranger-Moore, G. Body, and F. Tranquart, J. Ultrasound Med. **23**, 1629 (2004).
[10]M. Mitterberger, A. Pelzer, D. Colleselli, G. Bartsch, H. Strasser, L. Pallwein, F. Aigner, J. Gradl, and F. Frauscher, Eur. J. Radiol. **64**, 231 (2007).
[11]P. Phillips and E. Gardner, Eur. Radiol. Suppl. **14**, P4 (2004).
[12]P. J. Phillips, Ultrasonics Symposium (IEEE, 2001) (unpublished), p. 1739.
[13]J. Dave, F. Forsberg, D. A. Merton, S. Fernandes, T. B. Fox, L. M. Leodore, and A. L. Hall, *Ultrasonics Symposium*, (IEEE, 2008), p. 1655.
[14]F. Ching-Hsiang, Y. Chih-Kuang, H. Po-Hong, and L. Hao-Li, *Ultrasonics Symposium*, (IEEE, 2009), p. 1788.
[15]D. B. Ellegala, H. Leong-Poi, J. E. Carpenter, A. L. Klibanov, S. Kaul, M. E. Shaffrey, J. Sklenar, and J. R. Lindner, Circulation **108**, 336 (2003).
[16]R. E. Pollard, A. R. Broumas, E. R. Wisner, S. V. Vekich, and K. W. Ferrara, Ultrasound Med. Biol. **33**, 235 (2007).
[17]N. Lassau, L. Chami, B. Benatsou, P. Peronneau, and A. Roche, Eur. J. Radiol. **17**, F89 (2007).
[18]J. H. Zhou, W. Zheng, L. H. Cao, M. Liu, R. Z. Luo, F. Han, P. H. Wu, and A. H. Li, Br. J. Radiol. **84**, 826 (2011).
[19]P. -L. Lin, R. J. Eckersley, and E. A. H. Hall, Adv. Mater. **21**, 3949 (2009).
[20]H. P. Martinez, Y. Kono, S. L. Blair, S. Sandoval, J. Wang-Rodriguez, R. F. Mattrey, A. C. Kummel, and W. C. Trogler, Med. Chem. Commun. **1**, 266 (2010).
[21]H. Hu, H. Zhou, J. Du, Z. Wang, L. An, H. Yang, F. Li, H. Wu, and S. Yang, J. Mater. Chem. **21**, 6576 (2011).
[22]J. Lu, M. Liong, Z. Li, J. I. Zink, and F. Tamanoi, Small **6**, 1794 (2010).
[23]K. Shahani, S. K. Swaminathan, D. Freeman, A. Blum, L. Ma, and J. Panyam, Cancer Res. **70**, 4443 (2010).
[24]B. Urban-Klein, S. Werth, S. Abuharbeid, F. Czubayko, and A. Aigner, Gene Ther. **12**, 461 (2005).

[25]J. Zhang, M. Ding, F. Meng, M. Yuchi, and X. Zhang, Med. Phys. **38**, 4737 (2011).
[26]Y. Allusse, P. Horain, A. Agarwal, and C. Saipriyadarshan, Proceedings of the 16th ACM International Conference on Multimedia, 2008 (unpublished), pp. 1089–1092.
[27]F. Ino, J. Gomita, Y. Kawasaki, and K. Hagihara, *Parallel and Distributed Processing and Applications*, edited by M. Guo, L. Yang, B. Di Martino, H. Zima, J. Dongarra and F. Tang (Springer, Berlin, Germany, 2006), Vol. 4330, pp. 939–950.
[28]P. Bui and J. Brockman, Proceedings of 2nd Workshop on General Purpose Processing on Graphics Processing Units, 2009 (unpublished), p. 38.
[29]K. Hadinoto and W. S. Cheow, Drug Dev. Ind. Pharm. **35**, 1167 (2009).
[30]X. Lu, S. Zhang, H. Su, and Y. Chen, Comput. Med. Imaging Graph. **32**, 202 (2008).
[31]S. Butterworth, Wireless World **7**, 536 (1930).
[32]G. R. Arce and M. P. Mcloughlin, IEEE Trans. Acoust. Speech **35**, 60 (1987).